The Astrophysical Journal Letters, 768:L21 (5pp), 2013 May 1 doi:10.1088/2041-8205/768/1/L21

THE EFFECT OF SPATIAL GRADIENTS IN STELLAR MASS-TO-LIGHT RATIO ON BLACK HOLE MASS MEASUREMENTS

Nicholas J. McConnell[1], Shi-Fan Stephen Chen[2], Chung-Pei Ma[3], Jenny E. Greene[4], Tod R. Lauer[5], and Karl Gebhardt[6]
[1] Institute for Astronomy, University of Hawaii at Mānoa, Honolulu, HI, USA; nmcc@ifa.hawaii.edu
[2] Phillips Exeter Academy, Exeter, NH, USA
[3] Department of Astronomy, University of California at Berkeley, Berkeley, CA, USA; cpma@berkeley.edu
[4] Department of Astrophysics, Princeton University, Princeton, NJ, USA; jgreene@astro.princeton.edu
[5] National Optical Astronomy Observatory, Tucson, AZ, USA; lauer@noao.edu
[6] Department of Astronomy, University of Texas at Austin, Austin, TX, USA; gebhardt@astro.as.utexas.edu
Received 2013 February 24; accepted 2013 March 26; published 2013 April 19

ABSTRACT

We have tested the effect of spatial gradients in stellar mass-to-light ratio (Υ) on measurements of black hole masses ($M_\bullet$) derived from stellar orbit superposition models. Such models construct a static gravitational potential for a galaxy and its central black hole, but typically assume spatially uniform Υ. We have modeled three giant elliptical galaxies with gradients $\alpha \equiv d\log(\Upsilon)/d\log(r)$ from -0.2 to $+0.1$. Color and line strength gradients suggest mildly negative α in these galaxies. Introducing a negative (positive) gradient in Υ increases (decreases) the enclosed stellar mass near the center of the galaxy and leads to systematically smaller (larger) $M_\bullet$ measurements. For models with $\alpha = -0.2$, the best-fit values of $M_\bullet$ are 28%, 27%, and 17% lower than the constant-Υ case, in NGC 3842, NGC 6086, and NGC 7768, respectively. For $\alpha = +0.1$, $M_\bullet$ are 14%, 22%, and 17% higher than the constant-Υ case for the three respective galaxies. For NGC 3842 and NGC 6086, this bias is comparable to the statistical errors from individual modeling trials. At larger radii, negative (positive) gradients in Υ cause the total stellar mass to decrease (increase) and the dark matter fraction within one effective radius to increase (decrease).

Key word: galaxies: kinematics and dynamics

Online-only material: color figures

1. INTRODUCTION

Dynamical measurements of black hole masses ($M_\bullet$) at the centers of nearby galaxies have opened new avenues for studying galaxy evolution by exposing correlations between $M_\bullet$ and various host galaxy properties. Ongoing studies of these black hole scaling relations explore whether the growth and quenching of black holes and galaxies are causally linked or only loosely connected by broad trends in cosmic evolution. One way to improve on the determination of the black hole scaling relations and the cosmic scatter in $M_\bullet$ is to reduce uncertainties and systematic biases in measurements of $M_\bullet$ in local galaxies.

Among the approximately 70 nearby galaxies with dynamically determined $M_\bullet$, about 50 $M_\bullet$ have been measured using stellar kinematic data and orbit superposition models (McConnell & Ma 2013 and references therein). A number of assumptions made in the models can contribute to potential biases in the inferred black hole masses. Recent advances include modeling stellar mass and dark matter as separate components (e.g., Gebhardt & Thomas 2009), and accounting for triaxiality (e.g., van den Bosch & de Zeeuw 2010).

Another assumption that has been used in most previous orbit models is that the stellar mass-to-light ratio, Υ, is constant throughout a galaxy. This assumption is clearly a simplification since spatial gradients have been observed for many galaxy properties: e.g., color, metallicity, age, and α-element enhancement, which can all be associated with spatial variations in Υ. Early-type galaxies are often bluer toward their outer regions. Decreasing metallicity outward is likely the dominant cause for the color gradients in these galaxies (e.g., Strom et al. 1976; Tamura et al. 2000), with the age gradient playing a minor or insignificant role (e.g., Saglia et al. 2000; Tamura & Ohta 2004). This picture is supported by recent photometric studies of large statistical samples of early-type galaxies in the Sloan Digital Sky Survey (SDSS; Tortora et al. 2010a) as well as spectroscopic studies of individual galaxies (Spolaor et al. 2009; Rawle et al. 2010; Kuntschner et al. 2010). The spatial coverage of these studies is typically limited to the central regions of the galaxies within one effective radius ($r_{\rm eff}$). Measurements of 10 early-type galaxies have been extended to larger radii using deep observations with integral-field spectrographs (Weijmans et al. 2009; Greene et al. 2012). The central gradients in metallicity and absorption line strengths are seen to continue to 2–4 $r_{\rm eff}$. Gradients in color and inferred metallicity in galaxies' globular cluster systems persist to $\sim$8 $r_{\rm eff}$ (Arnold et al. 2011; Forbes et al. 2011).

Tight positive correlations between Υ and color have been found in both late-type and early-type galaxies (e.g., Bell & de Jong 2001; Bell et al. 2003; Tortora et al. 2011), with redder colors corresponding to larger Υ. By fitting synthetic spectral models to the observed optical color gradients, Tortora et al. (2011) have found mild negative gradients in Υ for local early-type galaxies with stellar ages >6 Gyr, over a large range of stellar masses ($M_\star \sim 10^{9.0}$–$10^{11.3}\ M_\odot$). Color and mass profiles have also been recently investigated in galaxies at $0.5 < z < 2.5$ (Szomoru et al. 2013).

In this Letter, we assess the amount of systematic error in $M_\bullet$ resulting from the standard assumption of constant Υ in the orbit models. We modify the orbit superposition code by Gebhardt et al. (2000) and introduce a spatial gradient in Υ to the stellar component of the potential. We investigate the effects on $M_\bullet$ for three giant elliptical galaxies that we have previously analyzed (assuming constant Υ): NGC 3842, NGC 6086, and NGC 7768 (McConnell et al. 2011a, 2011b,

2012). All three are massive ellipticals and brightest cluster galaxies (BCGs) with high stellar mass $M_\star$ and velocity dispersion σ: $M_\star = 1.55 \times 10^{12}, 1.43 \times 10^{12}, 1.16 \times 10^{12}\, M_\odot$, and $\sigma = 270, 318, 257\,\mathrm{km\,s^{-1}}$ for NGC 3842, NGC 6086, NGC 7768, respectively. The black hole masses were predominantly constrained by stellar kinematics from the integral-field spectrographs OSIRIS (Larkin et al. 2006) and GMOS (Allington-Smith et al. 2002; Hook et al. 2004) stellar kinematics at large radii were recorded with the Mitchell Spectrograph (Hill et al. 2008) or adopted from the literature (Carter et al. 1999; Loubser et al. 2008).

A few prior studies of $M_\bullet$ have explored variations in Υ. Recent investigations of S0 galaxies NGC 1332, NGC 3368, and NGC 3489 modeled bulge and disk components with separate Υ values (Nowak et al. 2010; Rusli et al. 2011). Nowak et al. (2007) assumed a separate Υ value for the nuclear disk in NGC 4486A. Gebhardt et al. (2000) assessed the $V-I$ color gradients in NGC 3379 and applied the corresponding Υ gradient to one set of models; Cappellari et al. (2002) applied a similar treatment to IC 1459. For both galaxies, models with a Υ gradient and models with uniform Υ yielded statistically consistent measurements of $M_\bullet$. Here, we extend from prior investigations by examining systematic trends in measured $M_\bullet$ over a range of Υ gradients.

2. STELLAR ORBIT MODELS AND Υ GRADIENTS

We use the axisymmetric orbit modeling algorithm of Gebhardt et al. (2000, 2003), Thomas et al. (2005), and Siopis et al. (2009). In this model, a galaxy is described by the density profile

$$\rho(r,\theta) = \Upsilon(r)\,\nu(r,\theta) + M_\bullet \delta(r) + \rho_{\rm dm}(r), \quad (1)$$

where $\nu(r,\theta)$ is the luminosity density derived from the galaxy's deprojected surface brightness profile and $\rho_{\rm dm}(r)$ represents a spherical Navarro–Frenk–White or cored logarithmic (LOG) dark matter profile. Equation (1) is used to construct a gravitational potential, and kinematic models of the galaxy are constructed by propagating test particles through the potential and computing their time-averaged velocities ("orbits") throughout a polar grid. Orbital weights are varied to fit the observed kinematics of the galaxy but are constrained such that the sum of weighted orbits exactly reproduces $\nu(r,\theta)$, which is decoupled from variations in $\Upsilon(r)$. The model velocity distributions are then compared to the observed kinematics, yielding a goodness-of-fit statistic χ^2. Each instance of the model adopts a single density profile and outputs a single χ^2 value. The best-fit values and confidence limits for $M_\bullet$ and other parameters in Equation (1) are determined by analyzing the distribution of χ^2 from many models.

Previous investigations using orbit superposition models typically have set $\Upsilon(r)$ to a uniform value, Υ_0. To assess the impact of a gradient in Υ, we set

$$\alpha = \frac{d\log\Upsilon}{d\log r}. \quad (2)$$

For each value of α, we sample a two-dimensional grid of values for $M_\bullet$ and the normalization of Υ.

The galaxies' color gradients indicate likely values of α. Figure 1 shows the color profile for each galaxy in our sample. The color gradients $\delta(B-R)/\delta(\log_{10} r)$ and $\delta(V-I)/\delta(\log_{10} r)$ range from -0.02 to -0.06. In Figure 2 of Tortora et al. (2011), the matching gradients in Υ are ≈ -0.1 to 0 for SDSS galaxies.

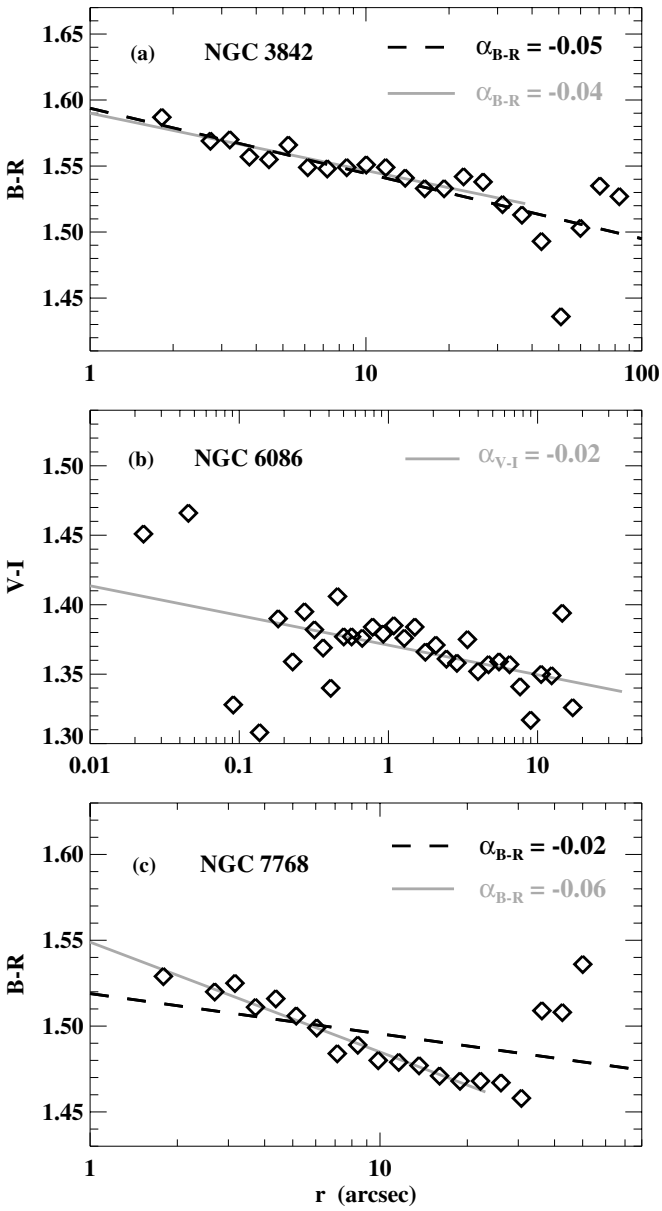

Figure 1. Color vs. radius in three giant elliptical galaxies based on photometric data from the *Hubble Space Telescope* and Kitt Peak National Observatory. In each panel, the black dashed line represents the best log-linear fit to all data points, and the solid gray line represents the best log-linear fit to data with $r \leqslant r_{\rm eff}$. For NGC 6086, our $V-I$ data extend to only $0.5\,r_{\rm eff}$ (17″). $B-R$ data from Peletier et al. (1990) extend to $1.2\,r_{\rm eff}$ and have a logarithmic slope of -0.06.

Their Figure 3 shows the Υ gradients as a function of stellar mass and velocity dispersion and indicates different mean values of α for galaxies with different stellar ages. Early-type galaxies with a central age older than 6 Gyr have $\alpha \sim -0.2$ to -0.1 over a large range of σ, but show a slight upturn toward $\alpha = 0$ at $M_\star > 10^{11}\, M_\odot$.

For NGC 3842, we have an additional 2 hr of on-source data from 2012 May observations with the Mitchell Spectrograph, allowing for a direct measurement of the Υ gradient. As described in detail in Greene et al. (2012), we construct elliptically averaged radial bins to maximize the signal-to-noise ratio (S/N) in the spectra. We have a median S/N of 40 per pixel in the largest bin, at $r \approx 1.1\,r_{\rm eff}$. First, weak emission features are iteratively corrected (Graves & Faber 2010) and velocity

Table 1
Results from Stellar Orbit Models

α	$M_\bullet$ ($10^9\,M_\odot$)	$\Upsilon(r_{\rm inf})$ ($\Upsilon_{\odot,R}$)	$\Upsilon(r_{\rm eff}/10)$ ($\Upsilon_{\odot,R}$)	$\Upsilon(r_{\rm eff})$ ($\Upsilon_{\odot,R}$)	$\langle\Upsilon\rangle$ ($\Upsilon_{\odot,R}$)
NGC 3842 ($r_{\rm inf} = 1\farcs2$; $r_{\rm eff} = 37\farcs8$; $D = 98.4$ Mpc)					
−0.2	$7.1^{+2.8}_{-2.8}$	$6.4^{+0.9}_{-0.9}$	$5.1^{+0.7}_{-0.7}$	$3.2^{+0.4}_{-0.4}$	$3.5^{+0.5}_{-0.5}$
−0.1	$8.7^{+2.9}_{-2.9}$	$5.8^{+0.8}_{-0.9}$	$5.1^{+0.7}_{-0.8}$	$4.1^{+0.6}_{-0.7}$	$4.3^{+0.6}_{-0.7}$
−0.05	$9.0^{+3.3}_{-2.5}$	$5.5^{+0.7}_{-0.8}$	$5.2^{+0.7}_{-0.8}$	$4.6^{+0.6}_{-0.7}$	$4.7^{+0.6}_{-0.7}$
0	$9.8^{+2.9}_{-2.5}$	$5.2^{+0.7}_{-0.7}$	$5.2^{+0.7}_{-0.7}$	$5.2^{+0.7}_{-0.7}$	$5.2^{+0.7}_{-0.7}$
0.05	$10.4^{+2.8}_{-2.5}$	$4.8^{+0.7}_{-0.7}$	$5.1^{+0.7}_{-0.7}$	$5.7^{+0.8}_{-0.8}$	$5.6^{+0.8}_{-0.8}$
0.1	$11.2^{+2.6}_{-2.8}$	$4.5^{+0.6}_{-0.6}$	$5.0^{+0.7}_{-0.7}$	$6.3^{+0.8}_{-0.9}$	$6.2^{+0.8}_{-0.9}$
0.2	$12.4^{+2.2}_{-2.6}$	$3.9^{+0.5}_{-0.6}$	$5.0^{+0.6}_{-0.7}$	$7.8^{+0.9}_{-1.2}$	$7.5^{+0.9}_{-1.1}$
NGC 6086 ($r_{\rm inf} = 0\farcs24$; $r_{\rm eff} = 36\farcs8$; $D = 139.1$ Mpc)					
−0.2	$2.6^{+1.5}_{-1.1}$	$6.1^{+0.5}_{-0.5}$	$3.6^{+0.3}_{-0.3}$	$2.2^{+0.2}_{-0.2}$	$2.8^{+0.2}_{-0.3}$
−0.1	$3.0^{+1.4}_{-1.1}$	$5.3^{+0.4}_{-0.4}$	$4.0^{+0.3}_{-0.3}$	$3.2^{+0.3}_{-0.3}$	$3.5^{+0.3}_{-0.3}$
0	$3.6^{+1.4}_{-1.2}$	$4.4^{+0.4}_{-0.4}$	$4.4^{+0.4}_{-0.4}$	$4.4^{+0.4}_{-0.4}$	$4.4^{+0.4}_{-0.4}$
0.1	$4.4^{+1.5}_{-1.3}$	$3.6^{+0.2}_{-0.3}$	$4.8^{+0.3}_{-0.4}$	$6.0^{+0.4}_{-0.5}$	$5.6^{+0.4}_{-0.5}$
NGC 7768 ($r_{\rm inf} = 0\farcs14$; $r_{\rm eff} = 23\farcs1$; $D = 112.8$ Mpc)					
−0.2	$1.0^{+0.5}_{-0.3}$	$7.5^{+1.2}_{-1.2}$	$4.3^{+0.7}_{-0.7}$	$2.7^{+0.4}_{-0.4}$	$2.7^{+0.4}_{-0.5}$
−0.1	$1.1^{+0.5}_{-0.3}$	$6.3^{+0.8}_{-0.9}$	$4.8^{+0.6}_{-0.7}$	$3.8^{+0.5}_{-0.6}$	$3.8^{+0.5}_{-0.6}$
0	$1.2^{+0.5}_{-0.3}$	$5.0^{+0.6}_{-0.5}$	$5.0^{+0.6}_{-0.5}$	$5.0^{+0.6}_{-0.5}$	$5.0^{+0.6}_{-0.5}$
0.1	$1.4^{+0.6}_{-0.3}$	$4.0^{+0.4}_{-0.5}$	$5.3^{+0.5}_{-0.6}$	$6.7^{+0.7}_{-0.8}$	$6.8^{+0.7}_{-0.8}$

Notes. Best-fit values and errors in $M_\bullet$ and Υ are the median values and 68% confidence limits derived from the cumulative likelihood method of McConnell et al. (2011b). Stellar mass-to-light ratios Υ are reported in R band. $\langle\Upsilon\rangle$ is the average luminosity-weighted value of Υ over the whole galaxy.

dispersions are measured at each bin using pPXF (Cappellari & Emsellem 2004). Then the stellar population properties are measured from the Lick_EW+EZ_Ages algorithm (Graves & Schiavon 2008). We use the $\alpha-$enhanced models of Schiavon (2007), assuming a Salpeter initial mass function (IMF), to determine the luminosity-weighted Υ at each radius. We find the resulting Υ gradient to be $\alpha = -0.13 \pm 0.30$, broadly consistent with the color gradient in NGC 3842. Uncertainties in the inner bins are dominated by systematic uncertainties in emission line and velocity dispersion measurements, while the outer bins include additional uncertainties from sky subtraction.

Gradients in the stellar IMF are potentially an additional source of Υ gradients within our galaxies. The IMF varies with the [Mg/Fe] line ratio and the corresponding inferred timescale for star formation (Conroy & van Dokkum 2012). Our line index measurements from Mitchell Spectrograph data of NGC 3842 are consistent with no radial gradient in [Mg/Fe]. Therefore, we do not expect IMF gradients to alter the likely range of α.

Given the uncertainties discussed above, we have chosen to test α ranging from −0.2 to 0.1. We employ α as a spherical, three-dimensional gradient in the models. Integrating our model stellar mass profiles along the line of sight, we find the projected gradients to be ≈80% of the three-dimensional α. The corresponding range of projected gradients, −0.16 to 0.08, is appropriate with regards to the inferred gradients from photometry and spectroscopy.

3. RESULTS

Table 1 and Figures 2 and 3 illustrate our best-fit values of $M_\bullet$ and Υ from modeling NGC 3842, NGC 6086, and NGC 7768

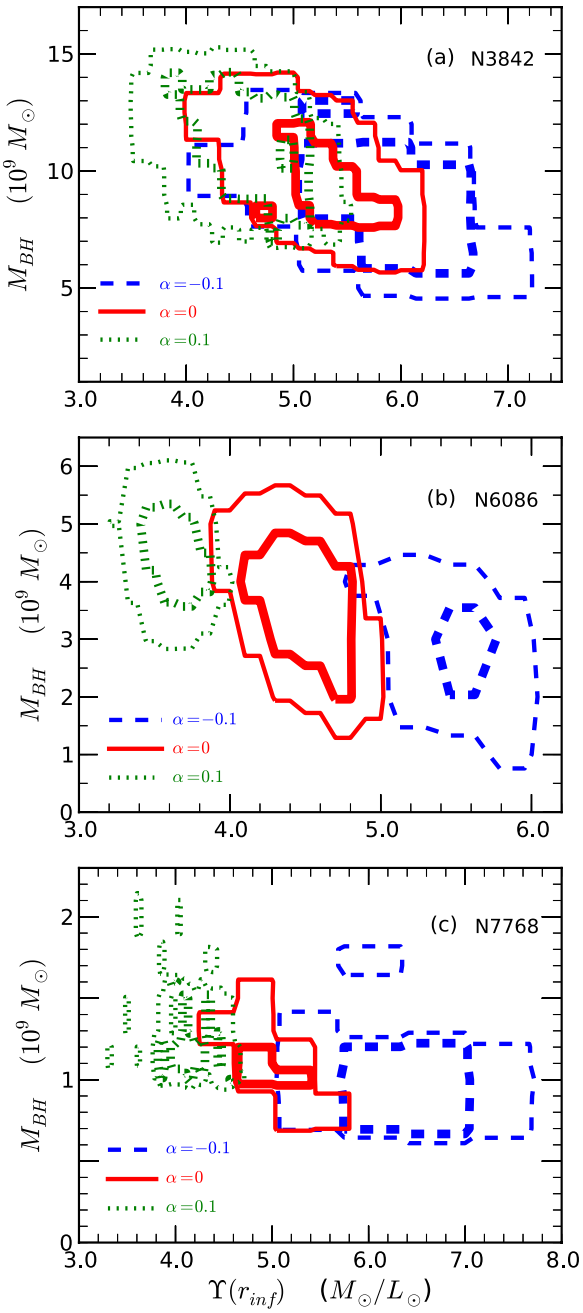

Figure 2. Contours of χ^2 as a function of $\Upsilon(r_{\rm inf})$ and $M_\bullet$, for orbit superposition models with different slopes for the logarithmic Υ gradient: $\alpha = -0.1$ (blue dashed), 0 (red solid), and +0.1 (green dotted). For each α, the thick and thin contours represent 68% and 90% confidence levels (corresponding to $\Delta\chi^2 = 1.0$ and 2.71), respectively.

(A color version of this figure is available in the online journal.)

with different index α for the Υ gradient. The stellar orbit models optimize the normalization of Υ, while the radial dependence is set by Equation (2) for fixed α. Each galaxy's distance D, effective radius $r_{\rm eff}$, and black hole radius of influence, $r_{\rm inf} \equiv GM_\bullet/\sigma^2$, are listed in Table 1. Since $r_{\rm inf}$ is much smaller than $r_{\rm eff}$ (with the ratio ranging from 0.006 to 0.03), we list Υ at three radii ($r_{\rm inf}$, $0.1\,r_{\rm eff}$, and $1\,r_{\rm eff}$) for comparison. We also list the average luminosity-weighted stellar mass-to-light ratio $\langle\Upsilon\rangle$, equal to the total stellar mass divided by the total luminosity.

Table 1 and Figure 2 show that within $r_{\rm inf}$, there is a mild degeneracy between stellar mass and black hole mass.

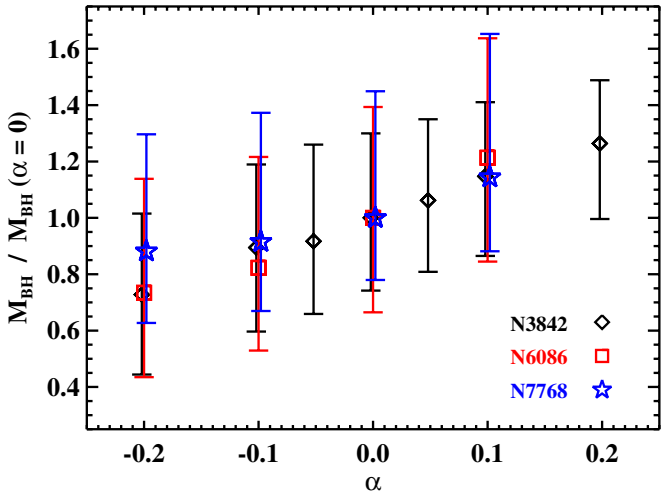

Figure 3. Best-fit $M_\bullet$ vs. Υ gradient α for models of NGC 3842, NGC 6086, and NGC 7768. The y-axis is the ratio of the best-fit $M_\bullet$ value relative to the best-fit value for models with uniform Υ ($\alpha = 0$). Error bars represent the statistical errors from individual trials (Table 1), also normalized relative to $M_\bullet(\alpha = 0)$.

(A color version of this figure is available in the online journal.)

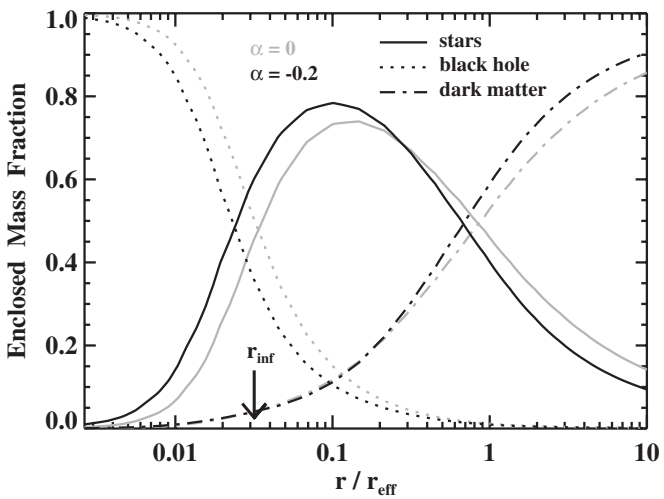

Figure 4. Enclosed mass fractions vs. deprojected radius for stars, dark matter, and a black hole, in the best-fit gravitational potential for NGC 3842. Two cases are shown: constant Υ ($\alpha = 0$; gray) and a Υ gradient with $\alpha = -0.2$ (black). The black hole dominates the mass at small radii within the sphere of influence $r_{\rm inf}$, stars dominate at intermediate radii of $r \sim 0.1\,r_{\rm eff}$, and the dark matter halo takes over at $r \gtrsim r_{\rm eff}$.

As α increases from negative toward positive values, $\Upsilon(r_{\rm inf})$ decreases, causing the best-fit $M_\bullet$ to increase. At large radii the trend with α is reversed, such that the best-fit $\Upsilon(r_{\rm eff})$ and $\langle\Upsilon\rangle$ both increase as α increases. The intermediate radius of $\sim 0.1\,r_{\rm eff}$ is roughly the pivot point at which the best-fit Υ has similar values for different α. Our kinematic data for each galaxy fall mainly within $1\,r_{\rm eff}$ and are most thoroughly represented at small radii ($r \lesssim 3''$, or $\sim 0.1\,r_{\rm eff}$), where the OSIRIS and GMOS integral-field spectrographs yield measurements at multiple position angles. This kinematic coverage drives the normalization of Υ, such that best-fitting models for each value of α have similar enclosed masses near $0.1\,r_{\rm eff}$ for a given galaxy. This is also the scale on which stars dominate the total enclosed mass: much within $\sim 0.1\,r_{\rm eff}$, the black hole begins to contribute, whereas the dark matter begins to dominate at ~ 0.5–$2\,r_{\rm eff}$ (Figure 4).

Figure 3 shows a clear positive correlation between α and the best-fit $M_\bullet$ value. As α decreases from 0 to -0.2, the best-fit $M_\bullet$ decreases by 28% in NGC 3842 and 27% in NGC 6086. For these galaxies, the bias in $M_\bullet$ over this range in α is comparable to the statistical uncertainty in $M_\bullet$ for each suite of models with fixed α. NGC 7768 exhibits a slightly smaller bias of 17% in $M_\bullet$, versus statistical uncertainties $\sim$40% from individual trials.

For each galaxy, the value of χ^2 for the best-fit model (for a given α) changes by less than 1.0 when α increases from -0.2 to 0. By contrast, χ^2 for the best-fit model increases by 2.5 as α increases from 0 to +0.2 for NGC 3842, and χ^2 increases by 1.0 and 2.8 for NGC 6086 and NGC 7768, respectively, as α increases from 0 to +0.1. Models with a positive gradient in Υ are therefore mildly disfavored by our kinematic data. This trend is consistent with the range of α inferred from the three galaxies' negative color gradients shown in Figure 1.

Figure 4 shows the relative contributions of stars, dark matter, and the black hole to the total enclosed mass as a function of deprojected radius in NGC 3842. Similar trends are seen for NGC 6086 and NGC 7768. For simplicity, we have modeled a single dark matter halo for each galaxy, for all values of α. As α decreases from 0 to -0.2, our kinematic data prefer a model with more (less) stellar mass at $r \ll 0.1\,r_{\rm inf}$ ($r \gg 0.1\,r_{\rm inf}$). Since we have assumed a fixed dark matter halo, the resulting enclosed stellar mass fraction is decreased at large radii.

If a range of dark matter profiles were sampled, we would expect changes in $\Upsilon(r)$ to alter the mass and/or shape of the best-fitting dark matter halo. Introducing a negative Υ gradient would redistribute stellar mass toward smaller radii, and the models could reconstruct the outer mass profile by fitting a more massive halo, amplifying the trend for dark matter in Figure 4. Our models are not sensitive to the inner slope of the dark matter profile, as the enclosed mass at small radii is dominated by stars and the black hole.

Since the dark matter halo and Υ gradient both cause a non-uniform *total* mass-to-light ratio, one might suspect that optimizing the dark matter profile for each value of α would decrease the variations in Υ normalization and $M_\bullet$. While our kinematic data for NGC 3842, NGC 6086, and NGC 7768 do not extend far enough to tightly constrain the dark matter profile, we have performed a simple test by varying α in models of NGC 3842 with no dark matter. Even without dark matter, the overall trend of Υ and $M_\bullet$ versus α is similar to those depicted in Figures 2(a) and 3.

4. DISCUSSION

We have run stellar orbit superposition models of three giant elliptical galaxies, assuming a range of gradients defined by $\alpha = d\log(\Upsilon)/d\log(r)$ in the stellar mass-to-light ratio Υ. We find that the best-fit black hole mass $M_\bullet$ varies systematically with the strength and sign of α. As α decreases from 0 to -0.2, the best-fit values of $M_\bullet$ decrease by 28%, 27%, and 17% for NGC 3842, NGC 6086, and NGC 7768, respectively. As α increases from 0 to +0.1, the best-fit values of $M_\bullet$ increase by 14%, 22%, and 17% for the three galaxies. For comparison, individual trials yield statistical errors $\sim$30%–40% in $M_\bullet$. Color and line strength gradients in these three galaxies suggest $\alpha \sim -0.2$ to -0.1.

Our results suggest that gradients in Υ may be a non-negligible source of systematic error in measurements of $M_\bullet$ and $M_\star$. The overall effect of this error on the correlations between $M_\bullet$ and host galaxy properties will depend on the distribution of Υ gradients across the sample of galaxies with existing $M_\bullet$ measurements.

All three galaxies in our study are BCGs with $M_\star > 10^{12}\,M_\odot$ and velocity dispersions $\sigma > 250\,\mathrm{km\,s^{-1}}$. Extrapolating the trend illustrated in Figure 3 to other values of α will indicate the potential level of bias in dynamical measurements of $M_\bullet$ that assume uniform Υ. A systematic variation in α with galaxy stellar mass or velocity dispersion can have an impact on the slopes of the $M_\bullet$–$M_{\rm bulge}$ and $M_\bullet$–σ scaling relations, which are currently determined assuming $\alpha = 0$ (e.g., McConnell & Ma 2013 and references therein). For early-type galaxies, Tortora et al. (2011) find a non-monotonic trend in the dependence of α on $M_\star$ and σ, where α has a minimum around $M_\star \sim 1$–$3 \times 10^{10}\,M_\odot$ ($\sigma \sim 100$–$160\ \mathrm{km\,s^{-1}}$) and increases mildly toward the low- and high-$M_\star$ (σ) ends. The scatter, however, is large. If α decreases (increases) with decreasing $M_{\rm bulge}$ or σ, our results here indicate that the inferred $M_\bullet$ would be systematically lower (higher) for smaller galaxies, thereby steepening (flattening) the slopes of the scaling relations. In some galaxies where kinematic measurements superbly resolve $r_{\rm inf}$, lower degeneracies between $M_\bullet$ and Υ will reduce systematic errors in $M_\bullet$.

In addition to biasing measurements of $M_\bullet$, gradients in Υ may impact other attempts to decompose mass profiles into multiple components. In particular, strong and weak lensing provide complementary data to stellar kinematics for probing the total mass profiles of galaxies and galaxy clusters. In contrast to our small-scale kinematic data for NGC 3842, NGC 6086, and NGC 7768, lensing studies typically constrain the total enclosed mass at larger radii of $\sim$1–100 $r_{\rm eff}$. In this case, the inner slope of the dark matter profile can be degenerate with the stellar mass profile. Current methods estimate the stellar mass component using stellar kinematics and/or population synthesis, under the assumption of spatially uniform Υ (e.g., Jiang & Kochanek 2007; Sand et al. 2008; Auger et al. 2010; Tortora et al. 2010b; Newman et al. 2011, 2013). Allowing for a gradient in Υ in these studies could affect the decomposition of the stellar and dark matter components. For instance, in the presence of a negative gradient in Υ, models sensitive to the enclosed mass slope near $1\,r_{\rm eff}$ might prefer a less cuspy dark matter profile to counteract the inward steepening in stellar mass.

Gravitational lensing is better suited for probing lensing galaxies at $z \sim 0.2$ and beyond, whereas direct dynamical measurements of $M_\bullet$ are currently feasible only in local galaxies within $\sim$150 Mpc. Other dynamical tracers such as globular clusters have been used to infer galaxy mass profiles out to several effective radii (e.g., Romanowsky et al. 2009; Murphy et al. 2011). A joint analysis combining the kinematics from our small-scale studies with those from the large-scale tracers can provide more comprehensive measurements of the mass profiles of stars and dark matter in early-type galaxies, from the black hole sphere of influence out to several effective radii.

This work was partially supported by NSF AST-1009663 and by a grant from the Simons Foundation (224959 to C.P.M.). N.J.M. is supported by the Beatrice Watson Parrent Fellowship. All models were run using facilities at the Texas Advanced Computing Center at the University of Texas at Austin. We thank Aaron Romanowsky for helpful discussions.

REFERENCES

Allington-Smith, J., Murray, G., Content, R., et al. 2002, PASP, 114, 892
Arnold, J. A., Romanowsky, A. J., Brodie, J. P., et al. 2011, ApJL, 736, L26
Auger, M. W., Treu, T., Gavazzi, R., et al. 2010, ApJL, 721, L163
Bell, E. F., & de Jong, R. S. 2001, ApJ, 550, 212
Bell, E. F., McIntosh, D. H., Katz, N., & Weinberg, M. D. 2003, ApJS, 149, 289
Cappellari, M., & Emsellem, E. 2004, PASP, 116, 138
Cappellari, M., Verolme, E. K., van der Marel, R. P., et al. 2002, ApJ, 578, 787
Carter, D., Bridges, T. J., & Hau, G. K. T. 1999, MNRAS, 307, 131
Conroy, C., & van Dokkum, P. G. 2012, ApJ, 760, 71
Forbes, D. A., Spitler, L. R., Strader, J., et al. 2011, MNRAS, 413, 2943
Gebhardt, K., Richstone, D., Kormendy, J., et al. 2000, AJ, 119, 1157
Gebhardt, K., Richstone, D., Tremaine, S., et al. 2003, ApJ, 583, 92
Gebhardt, K., & Thomas, J. 2009, ApJ, 700, 1690
Graves, G. J., & Faber, S. M. 2010, ApJ, 717, 803
Graves, G. J., & Schiavon, R. P. 2008, ApJS, 177, 446
Greene, J. E., Murphy, J. D., Comerford, J. M., Gebhardt, K., & Adams, J. J. 2012, ApJ, 750, 32
Hill, G. J., MacQueen, P. J., Smith, M. P., et al. 2008, Proc. SPIE, 7014, 701406
Hook, I. M., Jørgensen, I., Allington-Smith, J. R., et al. 2004, PASP, 116, 425
Jiang, G., & Kochanek, C. S. 2007, ApJ, 671, 1568
Kuntschner, H., Emsellem, E., Bacon, R., et al. 2010, MNRAS, 408, 97
Larkin, J., Barczys, M., Krabbe, A., et al. 2006, Proc. SPIE, 6269, 62691A
Loubser, S. I., Sansom, A. E., Sánchez-Blázquez, P., Soechting, I. K., & Bromage, G. E. 2008, MNRAS, 391, 1009
McConnell, N. J., & Ma, C.-P. 2013, ApJ, 764, 184
McConnell, N. J., Ma, C.-P., Gebhardt, K., et al. 2011a, Natur, 480, 215
McConnell, N. J., Ma, C.-P., Graham, J. R., et al. 2011b, ApJ, 728, 100
McConnell, N. J., Ma, C.-P., Murphy, J. D., et al. 2012, ApJ, 756, 179
Murphy, J. D., Gebhardt, K., & Adams, J. J. 2011, ApJ, 729, 129
Newman, A. B., Treu, T., Ellis, R. S., & Sand, D. J. 2011, ApJL, 728, L39
Newman, A. B., Treu, T., Ellis, R. S., & Sand, D. J. 2013, ApJ, 765, 25
Nowak, N., Saglia, R. P., Thomas, J., et al. 2007, MNRAS, 379, 909
Nowak, N., Thomas, J., Erwin, P., et al. 2010, MNRAS, 403, 646
Peletier, R. F., Davies, R. L., Illingworth, G. D., Davis, L. E., & Cawson, M. 1990, AJ, 100, 1091
Rawle, T. D., Smith, R. J., & Lucey, J. R. 2010, MNRAS, 401, 852
Romanowsky, A. J., Strader, J., Spitler, L. R., et al. 2009, AJ, 137, 4956
Rusli, S. P., Thomas, J., Erwin, P., et al. 2011, MNRAS, 410, 1223
Saglia, R. P., Maraston, C., Greggio, L., Bender, R., & Ziegler, B. 2000, A&A, 360, 911
Sand, D. J., Treu, T., Ellis, R. S., Smith, G. P., & Kneib, J.-P. 2008, ApJ, 674, 711
Schiavon, R. P. 2007, ApJS, 171, 146
Siopis, C., Gebhardt, K., Lauer, T. R., et al. 2009, ApJ, 693, 946
Spolaor, M., Proctor, R. N., Forbes, D. A., & Couch, W. J. 2009, ApJL, 691, L138
Strom, S. E., Strom, K. M., Goad, J. W., Vrba, F. J., & Rice, W. 1976, ApJ, 204, 684
Szomoru, D., Franx, M., van Dokkum, P. G., et al. 2013, ApJ, 763, 73
Tamura, N., Kobayashi, C., Arimoto, N., Kodama, T., & Ohta, K. 2000, AJ, 119, 2134
Tamura, N., & Ohta, K. 2004, MNRAS, 355, 617
Thomas, J., Saglia, R. P., Bender, R., et al. 2005, MNRAS, 360, 1355
Tortora, C., Napolitano, N. R., Cardone, V. F., et al. 2010a, MNRAS, 407, 144
Tortora, C., Napolitano, N. R., Romanowsky, A. J., & Jetzer, P. 2010b, ApJL, 721, L1
Tortora, C., Napolitano, N. R., Romanowsky, A. J., et al. 2011, MNRAS, 418, 1557
van den Bosch, R. C. E., & de Zeeuw, P. T. 2010, MNRAS, 401, 1770
Weijmans, A.-M., Cappellari, M., Bacon, R., et al. 2009, MNRAS, 398, 561